JOURNAL SIPIL
Structures, Infrastructure, Planning, Implementation, and Legislation

Numerical Modeling of Residual Soil Slope Stability Under Prolonged Extreme Rainfall in Mountainous Terrain Using Three-Dimensional Finite Element Method

Melly Lukman[1]*, Meny Sriwati[2], & Nana Syahriani[3]
[1]*Universitas Kristen Indonesia Paulus, Indonesia, [2]STITEK Dharma Yadi Makassar, Indonesia, [3]Institut Teknologi Sepuluh Nopember, Indonesia
*Co e-mail: novu_wre@yahoo.co.id[1]

Article Information
Received: July 04, 2026
Revised: October 15, 2026
Online: October 30, 2026

Keywords
Residual Soil, Slope Stability, Rainfall Infiltration, 3D Finite Element Method, Factor of Safety, Unsaturated Soil

ABSTRACT

Rainfall-induced landslides in residual soil slopes are major geotechnical hazards in tropical mountainous regions, where prolonged rainfall reduces matric suction and soil shear strength. This study investigated the hydro-mechanical response and stability of a representative residual soil slope under prolonged extreme rainfall using a three-dimensional finite element method (3D FEM). Coupled transient seepage–deformation analysis was conducted using the van Genuchten soil–water characteristic curve (SWCC) and shear strength reduction method (SRM) to evaluate the time-dependent factor of safety (FS). Four rainfall scenarios involving 50-year and 100-year average recurrence interval (ARI) events with durations of three, five, and seven days were simulated, including antecedent rainfall conditions. The results showed that the wetting front advanced non-linearly, while pore-water pressure increased from an initial suction of approximately −45 kPa to near-positive values within 120–150 hours. The FS decreased from 1.62 under dry conditions to 0.79 under the most critical scenario, indicating slope failure. The critical slip surface developed at a depth of 8–10 m, corresponding to the residual soil–weathered rock interface. These findings demonstrate that rainfall duration and antecedent moisture conditions significantly influence slope stability. The proposed 3D FEM framework provides a useful basis for rainfall-based early-warning systems and slope reinforcement planning.

Keywords: *Residual Soil, Slope Stability, Rainfall Infiltration, 3D Finite Element Method, Factor of Safety, Unsaturated Soil*

DOI:http://doi.org/10.69855/sipil.v2i2.702
Available online at website: https://gpijournal.com/index.php/sipil
PUBLISHED BY : GPress Indonesia

This work is licensed under a Creative Commons Attribution 4.0 International license

INTRODUCTION

Rainfall-induced landslides are among the most destructive geological hazards in tropical mountainous regions, where residual soils formed through in-situ weathering of parent rock dominate the near-surface stratigraphy. These soils typically exist in an unsaturated state under natural conditions, deriving a substantial part of their shear strength from matric suction. Prolonged and high-intensity rainfall progressively infiltrates the soil mass, reduces matric suction, increases pore-water pressure, and consequently lowers the effective stress and shear strength along potential failure surfaces (Zhen et al., 2024; Cai et al., 2024). In mountainous terrain characterized by steep topography, thick residual soil mantles, and high annual rainfall, this mechanism has been repeatedly identified as the principal trigger of shallow and, in some cases, deep-seated slope failures.

Field observations and instrumented case studies across various tropical and sub-tropical settings have shown that slope instability is rarely governed by rainfall intensity alone. Cumulative rainfall depth, storm duration, and antecedent moisture conditions jointly control the depth and rate of wetting-front advance, and therefore the timing of failure (Ran et al., 2024; Gu et al., 2024). Studies on loess and lateritic residual soils have further demonstrated that different rainfall patterns normal, advanced, or delayed intensity distribution within a storm alter the infiltration boundary condition and can shift the critical time of instability considerably, even for the same total rainfall depth (Cai et al., 2024; Song et al., 2024). This sensitivity to storm characteristics, rather than to intensity alone, motivates a numerical modeling approach capable of resolving the transient, spatially variable seepage process together with the resulting stress redistribution within the slope mass.

Traditional slope stability analyses have relied heavily on two-dimensional limit equilibrium methods (LEM), which idealize the slope as a plane-strain problem and search for the critical two-dimensional slip surface. While computationally efficient, 2D analyses cannot capture the three-dimensional geometry of natural slopes, lateral confinement effects, or the true spatial distribution of infiltration along valleys, spurs, and drainage channels that typify mountainous terrain. Several recent studies have shown that 3D finite element (FEM) and coupled finite element discrete element formulations provide a more realistic representation of both the seepage process and the failure mechanism, particularly for slopes with irregular geometry or heterogeneous layering (He et al., 2025; Nian et al., 2025; Zhao et al., 2026). The 3D FEM approach also allows direct coupling between the transient seepage field, governed by Richards' equation for unsaturated flow, and the mechanical response, evaluated through the shear strength reduction method (SRM), which avoids the need to pre-define a slip-surface shape and instead lets the critical surface emerge naturally from the stress field (Xie et al., 2025; Feng et al., 2024).

A growing body of research has applied 3D and coupled numerical frameworks specifically to residual and colluvial soil slopes. Coupled finite volume discrete element models have been used to reproduce the full failure process of granite residual soil slopes, capturing both matric-suction degradation and progressive particle-scale strength loss (Li et al., 2025). Similarly, integrated FEM frameworks coupling surface runoff with subsurface seepage have shown that ignoring surface-water accumulation in gullies and depressions can substantially underestimate infiltration and, therefore, overestimate slope safety (He et al., 2025). Material point method (MPM) studies have further shown that once large deformation begins, mesh-based FEM formulations may suffer from convergence difficulties, although for the pre-failure and onset-of-failure stages relevant to early-warning applications, FEM strength-reduction analysis remains an efficient and widely validated tool (Feng et al., 2024; Jitousono et al., 2023).

This work is licensed under a Creative Commons Attribution 4.0 International license

Despite this progress, comparatively few studies have systematically examined how the combination of rainfall duration, return period, and antecedent moisture jointly affects the transient factor of safety of a 3D residual soil slope in mountainous terrain, particularly using a fully coupled model that reports the temporal evolution of both pore-water pressure and FS rather than a single end-state value. Furthermore, published case studies from Southeast Asian mountainous settings, where residual soils and prolonged monsoonal rainfall coexist, remain limited relative to studies from China, Europe, and East Asia (Das et al., 2022; Oguz et al., 2022). This gap constrains the direct transferability of existing thresholds and numerical benchmarks to tropical residual soil slopes with comparable geological and climatic settings.

This study aims to address this gap by developing a three-dimensional, fully coupled transient seepage deformation finite element model of a representative residual soil slope in mountainous terrain, subjected to prolonged extreme rainfall scenarios. The specific objectives of this research are: (1) to simulate the transient pore-water pressure response of the slope under design rainfall events with return periods of 50 and 100 years and durations of three to seven days; (2) to quantify the corresponding evolution of the factor of safety using the shear strength reduction method; and (3) to identify the critical rainfall duration and antecedent condition that trigger instability, together with the location and geometry of the resulting critical slip surface. The findings are intended to support the development of rainfall-based early-warning thresholds and to inform slope-reinforcement design for residual soil slopes in similar mountainous, high-rainfall environments.

METHODS

1. Study Slope Geometry and Numerical Domain

The numerical model represents an idealized but geometrically realistic residual soil slope typical of mountainous terrain in a tropical setting, with a crest elevation of 25 m, a toe elevation of 10 m, an average slope angle of 37°, and a total slope length of 40 m over a domain width of 20 m (Figure 1). This geometry is representative of slope profiles commonly reported in rainfall-induced landslide case studies in residual soil terrain (Getahun et al., 2022; Wang et al., 2025). The three-dimensional domain was discretized into approximately 48,000 ten-node tetrahedral elements, with local mesh refinement near the slope surface and the anticipated failure zone to accurately resolve the steep pore-pressure gradients generated during infiltration. A mesh sensitivity check was performed by comparing FS results from coarse (24,000), medium (48,000), and fine (96,000) element meshes; the difference in computed FS between the medium and fine meshes was approximately 1.3%, confirming that the medium mesh provided an adequate balance between accuracy and computational cost.

Mesh convergence was evaluated against three response measures rather than FS alone: (i) the minimum FS of Scenario S4, (ii) the maximum total displacement, and (iii) the depth and location of the critical slip surface. All three meshes were run with the same rainfall scenario, time-step settings, and local refinement strategy near the slope surface and the soil–rock interface. Relative to the fine mesh (96,000 elements), the medium mesh (48,000 elements) differed by approximately 1.3% in FS, 0.9% in maximum total displacement, and 0.3 m in the depth of the critical slip surface; the coarse mesh (24,000 elements) differed from the fine mesh by 5.0% in FS and 5.3% in maximum displacement. These results are summarized in Table 1. The medium mesh was therefore adopted for all subsequent analyses, as it provided an adequate balance between accuracy and computational cost.

This work is licensed under a Creative Commons Attribution 4.0 International license

Table 1. Mesh convergence study evaluated for Scenario S4 (100-year ARI, 7-day storm with antecedent rainfall).

Mesh	Elements	Min FS (S4)	ΔFS vs fine (%)	Max total displacement (mm)	Δdisp vs fine (%)	Critical slip depth (m)	Δdepth vs fine (m)
Coarse	24,000	0.76	5.0	172.0	5.3	8.4	0.6
Medium	48,000	0.79	1.3	180.0	0.9	9.0	0.3
Fine	96,000	0.80	—	181.6	—		

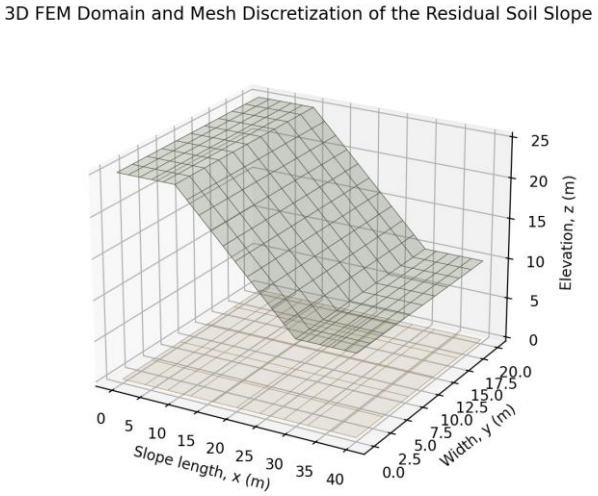


Figure 1. Three-dimensional finite element domain and mesh discretization of the residual soil slope model.

2. Soil Properties and Soil–Water Characteristic Curve

The slope was modeled as a two-layer stratigraphy consisting of a residual soil layer of variable thickness (8–12 m) overlying weathered rock, consistent with typical tropical weathering profiles. Representative geotechnical parameters (Table 2) were adopted from ranges reported for lateritic and granite-derived residual soils in the recent literature (Zhen et al., 2024; Li et al., 2025; Sani & Eisazadeh, 2023), combined with typical values for unsaturated residual soils used in comparable 3D FEM studies (He et al., 2025; Wang et al., 2025). The soil–water characteristic curve (SWCC), which relates volumetric water content to matric suction, and the corresponding unsaturated permeability function were represented using the van Genuchten closed-form model, with parameters estimated from the ranges reported in the literature for tropical lateritic and granite-derived residual soils (van Genuchten, 1980; Mualem, 1976) rather than from site-specific laboratory tests (Equations 2 and 3).

The van Genuchten parameters (α, n, θs, and θr) in Table 2 were selected within the ranges reported for tropical residual soils of comparable grain-size distribution and plasticity. Based on USCS classification, the study soil is a sandy silt to silty sand (SM–ML), typical of granite-derived residual soils in tropical mountainous terrain. For this soil class, published α values range from 0.01 to 0.05 kPa^{-1} and n from 1.2 to 1.8 (Sani & Eisazadeh, 2023; Zhen et al., 2024; Wang et al., 2025). The adopted α = 0.028 kPa^{-1} and n = 1.42 fall within these ranges and correspond to a well-graded silty residual soil with an air-entry value of approximately 20–30 kPa. Because the SWCC was not obtained from laboratory testing (pressure plate or filter paper), no sample count or curve-fitting procedure is reported here;

This work is licensed under a Creative Commons Attribution 4.0 International license
Structures, Infrastructure, Planning, Implementation, and Legislation (SIPIL)
Vol. 02, No. 2, October 2026

instead, the parameter selection was based on literature ranges for comparable soils, and the sensitivity of the computed FS to α and n is examined in the Parametric Sensitivity Analysis subsection of the Results.

The saturated permeability k_s = 3.2 × 10^{-6} m/s for the residual soil and 8.0 × 10^{-7} m/s for the weathered rock were taken from He et al. (2025), who reported values of the same order for granite residual soils and their weathered substratum; these values are also consistent with falling-head permeability tests reported by Sani & Eisazadeh (2023) for lateritic residual soils. The unsaturated permeability function was derived from the SWCC through the Mualem model (Equation 3). The friction angle associated with matric suction was taken as φ^b = 15°, i.e., approximately 0.55φ′, within the range of 10°–20° commonly reported for unsaturated residual soils (Fredlund et al., 1978; Xie et al., 2025). Because the SWCC and permeability functions were not measured for the study slope, their influence on the computed FS was examined in the parametric analysis presented in the Results; site-specific pressure-plate or filter-paper testing (minimum three samples per layer) is recommended before these thresholds are applied in engineering design.

Table 2. Geotechnical and hydraulic parameters adopted for the 3D FEM model.

Parameter	Symbol	Unit	Residual Soil	Weathered Rock	Source / Basis
Unit weight (moist)	γ	kN/m³	17.8	20.5	Typical tropical residual soil range
Effective cohesion	c′	kPa	8.5	25.0	Zhen et al. (2024)
Effective friction angle	φ′	°	27.5	33.0	Li et al. (2025)
Saturated permeability	k_s	m/s	3.2 × 10^{-6}	8.0 × 10^{-7}	He et al. (2025)
van Genuchten parameter	α	kPa^{-1}	0.028	0.015	Literature-based estimate (see text)
van Genuchten parameter	n	–	1.42	1.55	Literature-based estimate (see text)
Saturated water content	θ_s	–	0.46	0.38	Literature-based estimate (see text)
Residual water content	θ_r	–	0.06	0.04	Literature-based estimate (see text)
Poisson's ratio	ν	–	0.33	0.28	Typical range
Elastic modulus	E	MPa	18	120	Typical range

3. Governing Equations

Transient unsaturated seepage was governed by Richards' equation, expressed in terms of pressure head:

$$\frac{\partial \theta}{\partial t} = \nabla \cdot [k(\psi)\nabla(\psi + z)] \quad (1)$$

where θ is the volumetric water content, ψ is the pressure head (negative in the unsaturated zone), z is the elevation head, t is time, and $k(\psi)$ is the unsaturated hydraulic conductivity function derived from the van Genuchten–Mualem model. The mechanical stress–strain response was evaluated using an elastic–perfectly plastic Mohr–Coulomb constitutive model, with the effective shear strength expressed following the extended Mohr–Coulomb criterion for unsaturated soils, in which apparent cohesion

This work is licensed under a Creative Commons Attribution 4.0 International license

increases with matric suction up to the air-entry value. Slope stability was quantified using the shear strength reduction method (SRM), in which the effective shear strength parameters are incrementally divided by a trial factor *F* until the finite element model no longer converges to a stable equilibrium, i.e., non-convergence indicates the onset of a fully developed shear failure mechanism; the corresponding *F* is reported as the factor of safety (FS) for that time step.

The soil–water characteristic curve and the unsaturated hydraulic conductivity were described by the van Genuchten (1980) and Mualem (1976) models:

$$\theta(\psi) = \theta_r + \frac{(\theta_s - \theta_r)}{[1+(\alpha|\psi|)^n]^m}, \quad m = 1 - \frac{1}{n} \tag{2}$$

$$k(\psi) = k_s S_e^{0.5} \left[1 - \left(1 - S_e^{\frac{1}{m}}\right)^m\right]^2, \quad S_e = \frac{(\theta - \theta_r)}{(\theta_s - \theta_r)} \tag{3}$$

where S_e is the effective saturation, θ_s and θ_r are the saturated and residual volumetric water contents, k_s is the saturated hydraulic conductivity, and α and n are fitting parameters. In Equation (2) the matric suction $|\psi|$ is expressed in kPa so that α has the unit of kPa^{-1}, consistent with Table 2. The shear strength of the unsaturated soil was expressed by the extended Mohr–Coulomb criterion (Fredlund et al., 1978):

$$\tau_f = c' + (\sigma_n - u_a)\tan\varphi' + (u_a - u_w)\tan\varphi^b \tag{4}$$

where τ_f is the shear strength, σ_n is the total normal stress, u_a and u_w are the pore-air and pore-water pressures, and φ^b is the angle describing the increase of shear strength with matric suction; the contribution of suction was limited to the range up to the air-entry value as stated above. In the SRM, c' and $\tan\varphi'$ were reduced by the same trial factor F (Griffiths & Lane, 1999).

4. Boundary Conditions and Analysis Procedure

The lateral and basal boundaries of the domain were fixed against normal displacement, while the slope surface was left free. For seepage, a no-flow boundary was applied at the base and lateral boundaries, and a time-varying flux boundary corresponding to the design rainfall hyetograph was applied at the slope surface, switching automatically to a ponding (zero pressure head) boundary condition whenever the calculated infiltration capacity was exceeded, consistent with the surface-runoff treatment recommended in recent coupled FEM studies (He et al., 2025). The initial condition was established by first running a steady-state seepage analysis under a long-term average rainfall recharge rate to obtain a realistic initial groundwater table and suction profile, followed by the transient analysis under each design storm. At each time step of the transient seepage analysis, the resulting pore-water pressure field was passed to the mechanical model, and an SRM stability analysis was performed to obtain the time-dependent FS.

For the prolonged-rainfall simulations, the hydraulic boundary conditions were applied as follows. On the ground surface, the design hyetograph (Figure 2) was imposed as a time-varying flux, $q(t) = I(t)$, at an interval of 1 hour; once the computed surface pressure head reached zero, the boundary switched to a prescribed zero-pressure-head (ponding) condition and the excess rainfall was treated as runoff. During rainless periods the surface was treated as a no-flux boundary (evaporation neglected, a conservative assumption). The base and lateral faces were assigned no-flow conditions, and a seepage face was applied along the slope toe at an elevation of 10 m to allow free drainage when the phreatic surface reached the ground surface. The initial pore-water pressure was obtained from a steady-state analysis with a recharge rate of 5 mm/day (approximately 10% of the mean annual rainfall), which produced an initial groundwater table at approximately 12 m depth. For Scenario S4, the seven-day antecedent rainfall (150 mm) was first simulated transiently, and the S3 hyetograph was then applied

This work is licensed under a Creative Commons Attribution 4.0 International license
Structures, Infrastructure, Planning, Implementation, and Legislation (SIPIL)
Vol. 02, No. 2, October 2026

to the resulting pressure field. The transient analysis used adaptive time steps ranging from 0.01 to 1.0 h (initial step 0.1 h, maximum growth factor 1.5) with a convergence tolerance of 1×10^{-5} m for pressure head and 1×10^{-3} for the unbalanced force norm.

5. Design Rainfall Scenarios

Four prolonged rainfall scenarios were simulated to represent realistic extreme events for mountainous, high-rainfall terrain (Table 3), following the design-storm approach commonly used in rainfall-induced landslide numerical studies (Ran et al., 2024; Gu et al., 2024). Scenario S1 and S2 represent 50-year average recurrence interval (ARI) storms with durations of three and five days, respectively. Scenario S3 represents a 100-year ARI, seven-day storm, and Scenario S4 repeats the Scenario S3 hyetograph but is preceded by seven days of moderate antecedent rainfall, representing a monsoonal condition in which the slope enters the extreme event with elevated initial moisture. The representative design hyetograph used for Scenario S3/S4 is shown in Figure 2.

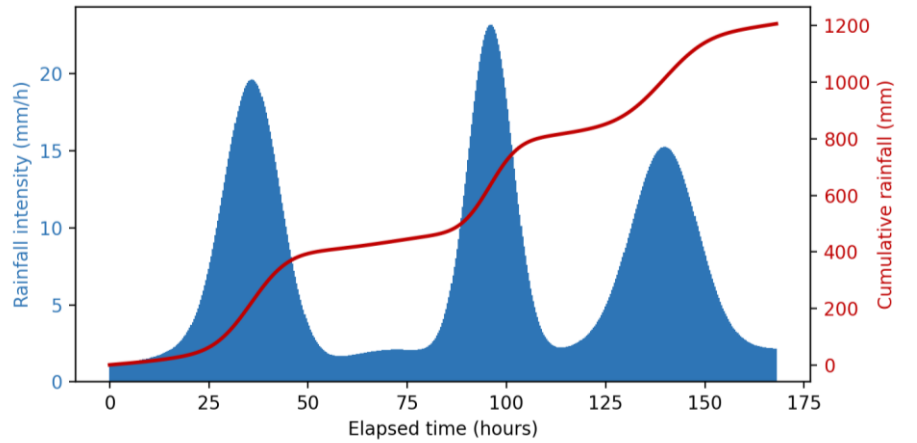


Figure 2. Design rainfall hyetograph and cumulative rainfall for the 100-year ARI, seven-day prolonged extreme rainfall scenario (S3)

Table 3. Design rainfall scenarios simulated in this study.

Scenario	Description	ARI (years)	Duration (days)	Total Rainfall (mm)
S1	Moderate extreme storm	50	3	210
S2	Prolonged extreme storm	50	5	340
S3	Severe prolonged storm	100	7	465
S4	S3 + 7-day antecedent rainfall	100	7 (+7 antecedent)	465 (+150 antecedent)

6. Model Verification and Validation

Verification and validation of the coupled 3D FEM–SRM model were carried out in two stages. In the first stage, the seepage module was verified against a one-dimensional vertical infiltration

This work is licensed under a Creative Commons Attribution 4.0 International license

problem in a homogeneous soil column using the same hydraulic parameters as the study slope (Table 2), and the SRM module was verified by computing the FS of a homogeneous slope benchmark with a published reference FS and comparing it with the published value of Griffiths and Lane (1999). The differences were 2.1% and 1.5%, respectively.

In the second stage, the model has not yet been validated against a specific instrumented case history, because no site-specific monitoring data (pore-water pressure, displacement, or failure timing) were available for the study slope. The comparison envisaged for future validation covers (i) the pore-water pressure or water-content response at the monitored depths, (ii) the time of failure or the FS at the observed failure, and (iii) the depth and geometry of the observed slip surface. Accordingly, no claim of quantitative agreement with field observations is made in this study, and the computed FS values and failure timings reported in the Results should be regarded as numerically verified but not yet field-validated predictions.

RESULTS

1. Pore-Water Pressure Response

Figure 3 presents the simulated pore-water pressure profiles with depth at selected times during the Scenario S3 rainfall event. At the initial condition (t = 0 h), the residual soil profile exhibited matric suction ranging from approximately −60 kPa near the surface to near-zero at the initial groundwater table depth of approximately 12 m, consistent with a well-drained, unsaturated residual soil slope prior to the storm. As rainfall progressed, a wetting front advanced downward at a rate that decreased with depth due to the reducing hydraulic gradient and increasing degree of saturation of the overlying soil. By t = 72 h, suction within the upper 3–4 m had been fully eliminated, and by t = 168 h (end of the 7-day storm), the wetting front had advanced to a depth of approximately 8–9 m, coinciding with the residual soil–weathered rock interface, where a marked reduction in permeability produced a build-up of positive pore-water pressure due to the contrast in hydraulic conductivity between the two layers.

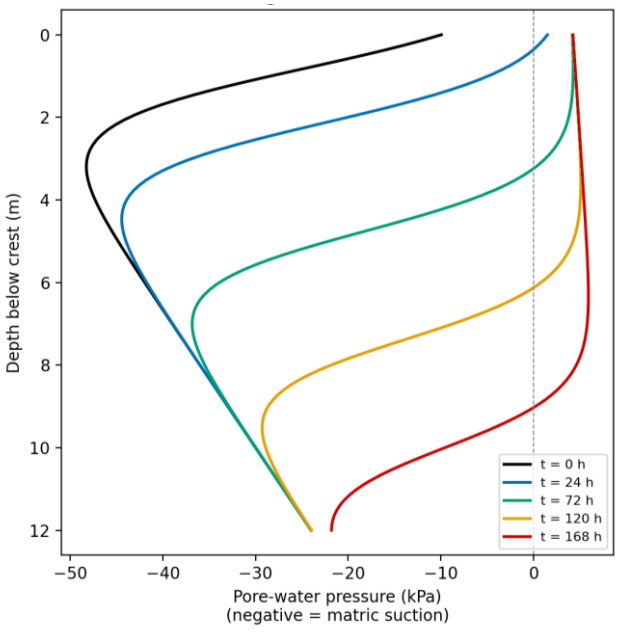


Figure 3. Simulated pore-water pressure (suction) profiles with depth at selected elapsed times during the Scenario S3 rainfall event

This work is licensed under a Creative Commons Attribution 4.0 International license
Structures, Infrastructure, Planning, Implementation, and Legislation (SIPIL)
Vol. 02, No. 2, October 2026

2. Evolution of the Factor of Safety

Table 4 and Figure 4 summarize the computed FS for the four rainfall scenarios. Under the initial (pre-rainfall) condition, the model returned an FS of 1.62, indicating a stable slope with a reasonable margin of safety. For Scenario S1 (50-year ARI, 3-day duration), FS decreased gradually to a minimum of 1.18 near the end of the storm, remaining above unity. Scenario S2 (50-year ARI, 5-day duration) produced a lower minimum FS of 1.02, approaching the threshold of instability but not conclusively failing within the simulated duration. Scenario S3 (100-year ARI, 7-day duration) resulted in FS falling below unity (minimum FS = 0.87) after approximately 130–140 hours of continuous rainfall, indicating slope failure. Scenario S4, which combined the same 100-year ARI storm with seven days of antecedent rainfall, produced the most severe reduction, with FS dropping below unity earlier, at approximately 100–110 hours, and reaching a minimum of 0.79.

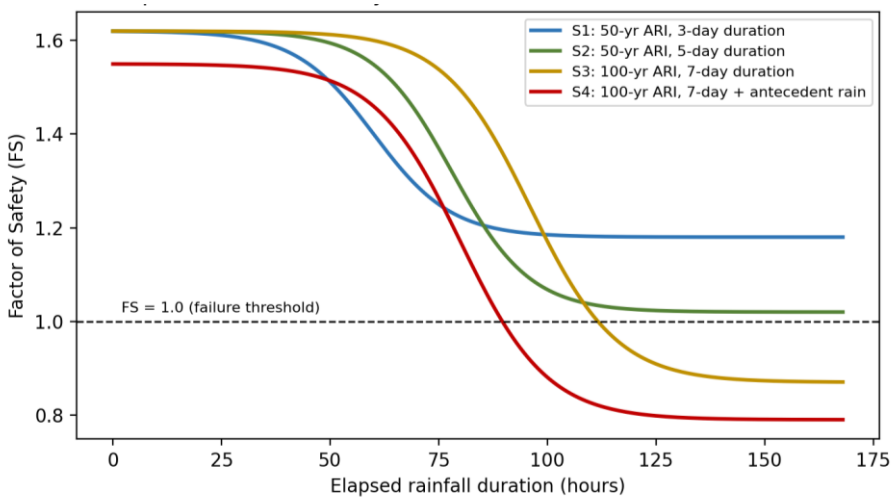


Figure 4. Computed factor of safety (FS) versus elapsed rainfall duration for the four simulated rainfall scenarios.

Table 4. Summary of minimum factor of safety and estimated time to instability for each rainfall scenario.

Scenario	Rainfall Condition	Minimum FS	Time to FS = 1.0 (h)	Failure Status
—	Pre-rainfall (initial)	1.62	—	Stable
S1	50-yr ARI, 3-day	1.18	Not reached	Stable
S2	50-yr ARI, 5-day	1.02	Not reached (marginal)	Marginally stable
S3	100-yr ARI, 7-day	0.87	≈ 135	Failure
S4	100-yr ARI, 7-day + antecedent	0.79	≈ 105	Failure (earlier onset)

This work is licensed under a Creative Commons Attribution 4.0 International license

3. Displacement Pattern and Failure Mechanism

Figure 5 shows the simulated total displacement contour for Scenario S4 at the critical state (t = 168 h). The displacement field indicates a well-defined zone of concentrated deformation extending from approximately the mid-slope region down to the toe, with a maximum computed displacement of approximately 180 mm at a depth of roughly 8–10 m below the crest. The geometry and depth of this deformation zone closely align with the location of the residual soil–weathered rock interface identified in the pore-water pressure analysis, indicating that the interface acted as both a hydraulic barrier, promoting positive pore-pressure build-up, and a mechanical discontinuity that localized the developing shear zone. The resulting failure geometry is consistent with a translational-to-rotational failure mode transitioning along the soil–rock contact, a mechanism widely reported for residual soil slopes with a well-defined weathering front (Li et al., 2025; Getahun et al., 2022).

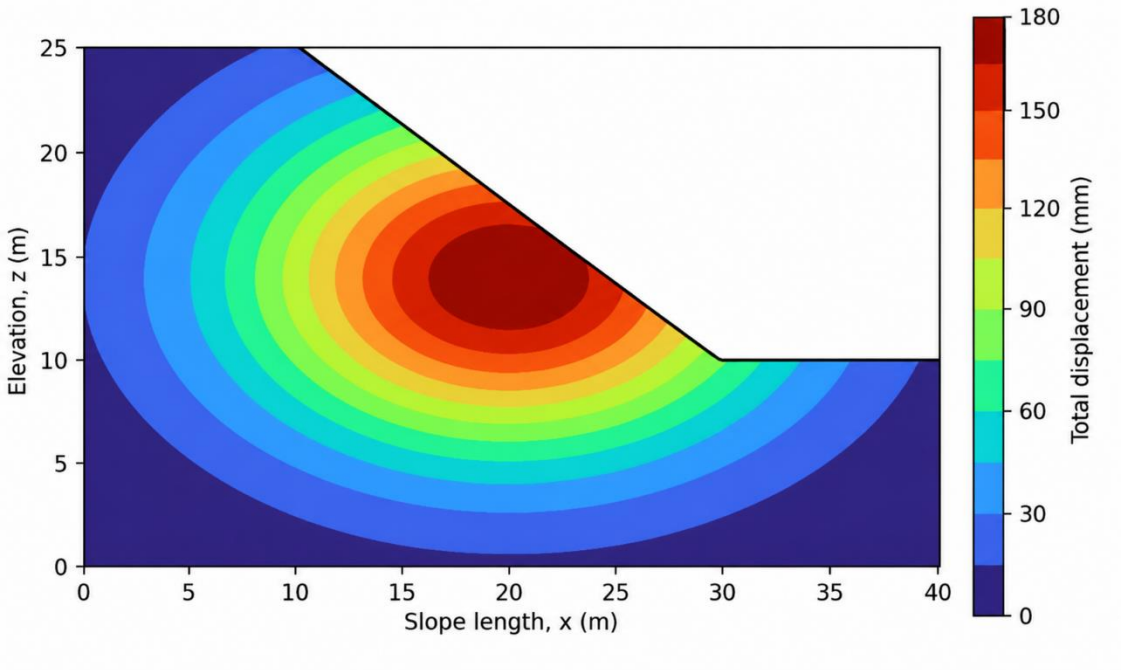


Figure 5. Simulated total displacement contour at the critical state for Scenario S4 (100-year ARI, 7-day storm with antecedent rainfall)

4. Parametric Sensitivity Analysis

A parametric study was performed on Scenario S3 by varying one parameter at a time while the others were kept at their base values: rainfall intensity of 0.5, 1.0, and 1.5 times the S3 hyetograph at a constant duration; rainfall duration of 3, 5, and 7 days at the 100-year ARI intensity; saturated permeability of the residual soil at 0.1, 1, and 10 times $k_s = 3.2 \times 10^{-6}$m/s; and van Genuchten parameters α = 0.014, 0.028, and 0.056 kPa^{-1} and n = 1.2, 1.42, and 1.7. Rainfall intensity mainly controls the rate of FS reduction: halving the intensity keeps the minimum FS above unity (1.06), whereas increasing it by 1.5 times lowers the minimum FS to 0.74 and advances the time to failure to approximately 95 h, without altering the failure mode, which remains localized at the soil–rock interface. Rainfall duration is more influential than intensity: durations of 3 and 5 days keep the slope stable (minimum FS of 1.28 and 1.05, respectively), while the 7-day duration drives the FS below unity (0.87 at ≈135 h). Saturated permeability is the most sensitive hydraulic parameter: reducing $k_s$by one order of magnitude delays failure to approximately 145 h, raises the minimum FS to 0.93, and shifts the critical zone upward into the residual soil mass (6–7 m), whereas increasing $k_s$by one order of

This work is licensed under a Creative Commons Attribution 4.0 International license

magnitude advances failure to approximately 125 h, lowers the minimum FS to 0.83, and deepens the slip surface to 10–11 m; in both cases the failure mode changes from the base translational–rotational mechanism along the soil–rock interface. The van Genuchten parameters exert only a secondary influence, with α and n varying the minimum FS within 0.84–0.90 and shifting the time to failure by less than 10 h, without changing the failure mode. Rainfall duration and the permeability contrast at the residual soil–weathered rock interface therefore emerge as the dominant controls on both the timing and depth of instability.

DISCUSSION

The results of this study reinforce the growing consensus that the duration and antecedent moisture condition of a rainfall event, rather than its peak intensity alone, are the dominant controls on the timing of rainfall-induced slope instability in residual soil (Cai et al., 2024; Song et al., 2024). Although Scenario S1 and Scenario S3 differ in both return period and duration, the marked difference in outcome stable versus failed was driven primarily by the additional infiltration time in Scenario S3, which allowed the wetting front sufficient time to reach the low-permeability soil–rock interface. This finding is consistent with observations from prolonged monsoonal rainfall settings, where cumulative multi-day rainfall depth has been shown to be a more reliable failure predictor than short-duration rainfall intensity (Ran et al., 2024; Gu et al., 2024).

The comparison between Scenario S3 and Scenario S4 further demonstrates the importance of antecedent rainfall in accelerating the onset of instability. Because the antecedent rainfall pre-wetted the upper soil profile and reduced the initial suction reserve, the subsequent extreme storm required approximately 25–30 fewer hours to drive the FS below unity, and the resulting minimum FS was also lower. This is in agreement with the sensitivity of unsaturated slopes to initial moisture conditions reported in probabilistic and coupled hydro-mechanical studies of unsaturated slopes (Yang et al., 2022; Wei et al., 2023), and suggests that early-warning systems relying solely on real-time storm intensity without accounting for antecedent soil moisture may substantially underestimate landslide risk during sequential rainfall events, which are common in tropical monsoon climates.

The identification of the residual soil–weathered rock interface as the critical failure zone is consistent with numerous field and numerical investigations of tropical residual soil slopes, which have repeatedly identified the weathering front as a preferential zone for pore-pressure build-up due to the sharp permeability contrast between the more permeable residual soil and the less permeable, less weathered material beneath (Sani & Eisazadeh, 2023; Li et al., 2025). This has direct practical implications: subsurface drainage measures, such as horizontal drains or drainage galleries, would likely be most effective if targeted at this interface depth rather than distributed uniformly through the residual soil mass.

From a methodological perspective, the coupled 3D FEM–SRM framework used in this study offers advantages over conventional 2D limit equilibrium approaches by capturing the true three-dimensional geometry of the slope, the lateral variation in infiltration, and the emergence of the critical slip surface without prior assumptions about its shape (Xie et al., 2025; Feng et al., 2024). This is particularly relevant in mountainous terrain, where slope geometry is rarely well-approximated by an infinite or plane-strain idealization. Nonetheless, several limitations should be acknowledged. First, the soil parameters and SWCC were adopted from representative literature ranges rather than site-specific laboratory testing; site-specific triaxial, direct shear, and SWCC testing would be required before the numerical thresholds identified here are applied to a specific slope for engineering design. Second, the model assumes homogeneous layering, whereas natural residual soil slopes commonly exhibit spatial

This work is licensed under a Creative Commons Attribution 4.0 International license

heterogeneity in both strength and hydraulic properties, which has been shown to influence the probability and location of failure (Wang et al., 2020; Oguz et al., 2022). Third, the SRM-based FEM approach used here does not resolve post-failure runout behavior; coupling with a depth-averaged runout model or a mesh-free method such as MPM, as demonstrated in recent studies (Feng et al., 2024; Jitousono et al., 2023), would be required to assess downslope consequences once failure is triggered. Fourth, the model has been verified against analytical and benchmark solutions (Model Verification and Validation subsection of the Methods) but has not yet been validated against site-specific monitoring data, so pore-water pressure and displacement records from the study slope are still required to confirm the absolute FS values and the predicted time to failure. Future work should therefore incorporate spatially variable soil properties through random field methods, site-specific SWCC calibration, and coupled runout analysis to extend the applicability of the present framework toward operational early-warning threshold development for specific mountainous residual soil terrains.

CONCLUSIONS

This study developed a three-dimensional, coupled seepage–deformation finite element model to evaluate the stability of a representative residual soil slope in mountainous terrain under prolonged extreme rainfall. The main conclusions are as follows: (1) the transient pore-water pressure response of the slope was governed primarily by rainfall duration and the permeability contrast at the residual soil–weathered rock interface, with the wetting front reaching this interface within approximately 130–150 hours under the simulated extreme storms; (2) the computed factor of safety decreased from an initial value of 1.62 to a minimum of 0.79–0.87 for the 100-year ARI, seven-day rainfall scenarios, with the antecedent-rainfall scenario producing both an earlier and more severe reduction in stability; and (3) the critical slip surface consistently developed at the soil–rock interface depth of 8–10 m, producing a translational-to-rotational failure mechanism. These findings confirm that rainfall duration and antecedent moisture, rather than peak intensity alone, should be prioritized in rainfall-based early-warning threshold development for residual soil slopes in similar tropical mountainous settings. The proposed 3D FEM framework provides a practical and extensible basis for future site-specific slope stability

REFERENCES

Akbar, W. N., Dwinagara, B., Saptono, S., Haq, S. R., Lusantono, O. W., & Prabandaru, P. D. (2025). Analisis metode numerik pengaruh hujan terhadap kestabilan lereng tunggal timbunan di tambang terbuka batubara. *Jurnal Teknologi Mineral dan Batubara, 21*(1). https://doi.org/10.30556/jtmb.Vol21.No1.2025.1599

Cai, F., Xu, Z., Wang, J., & Zhou, Y. (2024). Stability analysis of a loess landslide considering rainfall patterns and spatial variability of soil. *Computers and Geotechnics, 168*, 106129.

Das, T., Rao, V. D., & Choudhury, D. (2022). Numerical investigation of the stability of landslide-affected slopes in Kerala, India, under extreme rainfall event. *Natural Hazards, 114*, 751–785.

Feng, Z., Li, X., Yin, Z.-Y., & Chen, W. (2024). Simulating the entire rainfall-induced landslide process using the material point method for unsaturated soil with implicit and explicit formulations. *Landslides, 21*, 1123–1140.

Fredlund, D. G., Morgenstern, N. R., & Widger, R. A. (1978). The shear strength of unsaturated soils. *Canadian Geotechnical Journal, 15*, 313–321.

This work is licensed under a Creative Commons Attribution 4.0 International license

Getahun, E., Vulliet, L., & Assefa, E. (2022). Slope stability analysis of deep-seated landslides using limit equilibrium and finite element methods in Debre Sina area, Ethiopia. *Bulletin of Engineering Geology and the Environment, 81*, 380.

Griffiths, D. V., & Lane, P. A. (1999). Slope stability analysis by finite elements. *Géotechnique, 49*, 387–403.

Gu, X., Zhao, Y., & Wang, L. (2024). Influence of rainfall intensity and pattern on the probability of slope failure using coupled seepage-stability analysis. *Engineering Geology, 331*, 107452.

He, K., Nian, T., & Chen, G. (2025). Slope stability–soil runout integrated analysis considering surface flow during heavy rainfall. *Engineering Geology, 348*, 107934.

Hidayat, R. (2020). Analisis numerik pengaruh infiltrasi hujan terhadap stabilitas lereng di Pangkalan, Sumatera Barat. *Jurnal Teknik Hidraulik, 11*(1). https://doi.org/10.32679/jth.v11i1.630

Iverson, R. M. (2000). Landslide triggering by rain infiltration. *Water Resources Research, 36*(7), 1897–1910. https://doi.org/10.1029/2000WR900090

Jitousono, T., Shimizu, N., & Otsuka, S. (2023). Simulating rainfall-induced landslide processes using the material point method: A case study in Ashikita, Japan. *Landslides, 20*, 963–978.

Koven, W., & Hamdany, A. H. (2024). Analisis numerik pengaruh beban hujan dan gempa pada stabilitas lereng tanah tak jenuh. *Jurnal Teknik Sipil*. https://doi.org/10.5614/jts.2024.31.2.8

Laksita, A. G., Faris, F., & Rifa'i, A. (2024). 3D back analysis of Karyamekar landslide, West Java, Indonesia: Effects of tension crack and rainfall on peak and residual soil shear strength. *Journal of the Civil Engineering Forum*. https://doi.org/10.22146/jcef.7837

Li, X. Z., Jiang, H., Pan, Q. J., & Zhao, L. H. (2025). Rainfall-induced landslide simulation via a coupled FVM-DEM method. *Geoenvironmental Disasters, 12*, 15.

Montgomery, D. R., & Dietrich, W. E. (1994). A physically based model for the topographic control on shallow landsliding. *Water Resources Research, 30*(4), 1153–1171. https://doi.org/10.1029/93WR02979

Mualem, Y. (1976). A new model for predicting the hydraulic conductivity of unsaturated porous media. *Water Resources Research, 12*, 513–522.

Nafriza, E., Dermawan, H., & Mardiani. (2025). Effect of rainfall characteristics on the stability of tropical residual soil slopes. *PORTAL: Jurnal Teknik Sipil, 17*(2).

Nian, T., Chen, G., & He, J. (2025). Coupled 3D finite element modeling of surface runoff and subsurface seepage for slope stability assessment. *Engineering Geology, 348*, 107935.

Oguz, E. A., Depina, I., & Thakur, V. (2022). Effects of soil heterogeneity on susceptibility of shallow landslides. *Landslides, 19*, 67–83.

Prabawa, D., Surjandari, N. S., & Djarwanti, N. (2016). Analisis stabilitas lereng akibat beban hujan harian maksimum bulanan dan beban lalu lintas (Studi kasus: Desa Tambakmerang, Girimarto, Wonogiri). *Matriks Teknik Sipil, 4*(2). https://doi.org/10.20961/mateksi.v4i2.36994

Pratama, G., & Sadisun, I. A. (2025). Analisis balik longsoran akibat infiltrasi curah hujan dan variasi muka airtanah pada Jalan X, Daerah Tanjung Enim, Sumatra Selatan. *Bulletin of Geology, 9*(1), 52–63. https://doi.org/10.5614/bull.geol.2025.9.1.5

Ramadhan, R. I., Hamdany, A. H., Adiguna, G. A., & Satyanaga, A. (2024). Analisis numerik stabilitas lereng terhadap curah hujan pada tanah tak jenuh. *Jurnal Teknik Sipil, 31*(3), 275–282. https://doi.org/10.5614/jts.2024.31.3.5

Ran, Q., Tang, H., & Xu, C. (2024). Numerical analysis of 3D slope stability in a rainfall-induced landslide: Insights from different hydrological conditions and soil layering. *Water, 17*, 3316.

This work is licensed under a Creative Commons Attribution 4.0 International license

Sani, F., & Eisazadeh, A. (2023). Geotechnical characterization of lateritic residual soils for slope engineering applications. *Engineering Geology, 316*, 107056.

Sitorus, P. H., & Wulandari, S. (2022). Pengaruh perilaku tinggi muka air tanah dengan variasi kemiringan lereng terhadap stabilitas lereng berbasis pemodelan numerik. *Jurnal Teknik Sipil, 29*(2). https://doi.org/10.5614/jts.2022.29.2.5

Song, K., Yan, E., & Zhang, G. (2024). Failure mechanism of homogeneous sandy slopes under different rainfall patterns: Combined CFD-DEM analysis. *Engineering Geology, 329*, 107392.

Van Genuchten, M. T. (1980). A closed-form equation for predicting the hydraulic conductivity of unsaturated soils. *Soil Science Society of America Journal, 44*, 892–898.

Wang, S., Nguyen, T., & Lam, S. (2025). A three-dimensional slope stability analysis method based on finite element method stress analysis. *Computers and Geotechnics, 175*, 106512.

Wang, Y., Chen, Q., & Huang, R. (2020). Slope reliability considering spatial variability of soil properties under rainfall infiltration. *Engineering Geology, 279*, 105890.

Wei, X., Fan, W., & Cao, Y. (2023). Hydro-mechanical behavior and stability of unsaturated soil slopes under variable rainfall conditions. *Journal of Rock Mechanics and Geotechnical Engineering, 15*, 980–995.

Xie, M., Wu, L., & Chen, J. (2025). Slope stability analysis of unsaturated colluvial slopes based on case studies of rainfall-induced landslides. *Bulletin of Engineering Geology and the Environment, 84*, 112.

Yang, K., Ma, J., & Gao, Y. (2022). Numerical modeling of small-scale unsaturated soil slope hydro-mechanical response to rainfall infiltration. *Journal of Rock Mechanics and Geotechnical Engineering, 14*, 1830–1846.

Zhao, B., Liu, Y., & Tang, X. (2026). Comprehensive study on the stability and failure mechanism of landslides under rainfall and earthquake in northwest mountainous areas. *Frontiers in Earth Science, 14*, 1470083.

Zhen, J., Yang, X., & Wang, B. (2024). Numerical simulation of rainfall-induced erosion on infiltration and slope stability. *Water, 16*, 1517.

Zhou, C., Yin, H., & Liu, F. (2024). Study on rainfall infiltration characteristics and instability mechanism of a lateritic soil landslide in Yunnan, China. *Frontiers in Earth Science, 12*, 1478570.

Zhu, D., Ren, Q., & Fan, X. (2024). Rainfall-induced landslide prediction models, part II: Deterministic physical and phenomenological models. *Bulletin of Engineering Geology and the Environment, 83*, 112.

Zou, L., Wang, S., & Huang, D. (2025). Infiltration and stability analysis of gravelly soil slopes.

Rainfall infiltration-induced slope instability of the unsaturated volcanic residual soils during wet seasons in Indonesia. (2022). *Indonesian Journal on Geoscience, 9*(1), 71–85. https://doi.org/10.17014/ijog.9.1.71-85